doi:10.14311/ppt.2026.1.7
Plasma Physics and Technology **13**(1):7–12, 2026

SIMULATION OF CONTACTOR FOR REGIONAL HYBRID-ELECTRIC AIRCRAFT

B. Barbu*, F. Berger

Faculty of Electrical Engineering, Technische Universität Ilmenau, Gustav-Kirchhoff 1, 98693, Germany

* bogdan.barbu@tu-ilmenau.de

Abstract. To meet the decarbonization objectives set forth by the European Union, the aerospace sector is engaged in the development of a novel category of regional hybrid aircraft that integrates advanced DC technologies alongside conventional systems. This publication presents the proposed direct current (DC) system of the next-generation hybrid aircraft focusing on one of the protection elements developed for the kilo-volt DC (KHVDC) network, namely a mechanical contactor. The contactor design, its key characteristics as well as the chosen numerical model are presented and discussed in detail. The magnetohydrodynamics (MHD) model, details and focuses on a solution that integrates two distinct Ansys software packages, Fluent and Electronics Desktop (Maxwell 3D), chosen to enhance the electric arc modeling in non-linear magnetic environments. The qualitative results obtained from the numerical model will be discussed against experimental observations.

Keywords: hybrid airplane, KHVDC, contactor, simulation.

1. Introduction

The reduction of Greenhouse Gas (GHG) emissions and other pollutants is a critical objective for the aviation industry. Driven by the environmental targets set forth by the European Union, which must be integrated into the prospective development of the aeronautics market, the transition towards a more-electric aircraft is already underway on some of the existing airplane models. Nevertheless, to comply with the -30% net GHG emissions reduction by 2035 imposed by EU, additional measures are required. The Hybrid Electric Regional Aircraft Distribution Technologies (HECATE) project [1], part of the Clean Aviation program, aims to develop certifiable electric distribution systems and components capable of enabling the next step in airplane electrification, namely the hybrid-electric propulsion for regional airplanes. The systems and their components must reach TRL5 by the end of 2025 and should allow good scalability for future development. The chosen electrical architecture [2], schematically represented in Figure 1, is developed to work with direct currents (DC) and comprises 3 voltage levels: the KHVDC level at 800 V_{DC} is foreseen for propulsion and distribution, the HVDC at 540 V_{DC} is reserved for high-power non-propulsive loads and the LVDC level at 28 V_{DC} will be used to supply all conventional loads on the plane.

The protection of the KHVDC system is provided by an integrated solution where several smart electromechanical devices are coordinated to cut-off the current according to a predefined sequence. The system monitoring and device trigger sequence are ensured by an integrated electronic control unit. Although the complete layout and components of the KHVDC network are still under development, short circuit currents of up to 10 kA are expected to occur in the worst-case scenario. The following sections will present the contactor design, detail the numerical model and its assumptions, and discuss the preliminary results of this research.

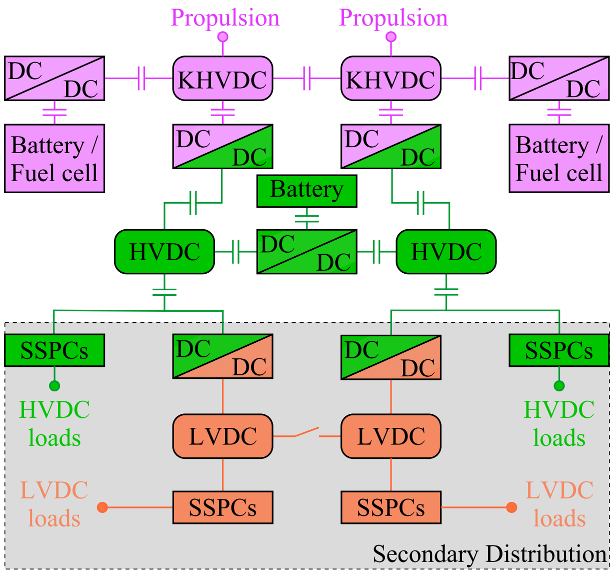

Figure 1. Chosen electrical arhitecture for hybrid-electric regional airplanes in project HECATE [2]

2. Contactor design and experimental setup

The contactor developed for the KHVDC level protection is presented in a simplified manner in Figure 2. The architecture of the device was developed to consider the conditions imposed by a DC switch-off procedure. In this context, the lack of a current-zero crossing along with the anticipated high short-circuit

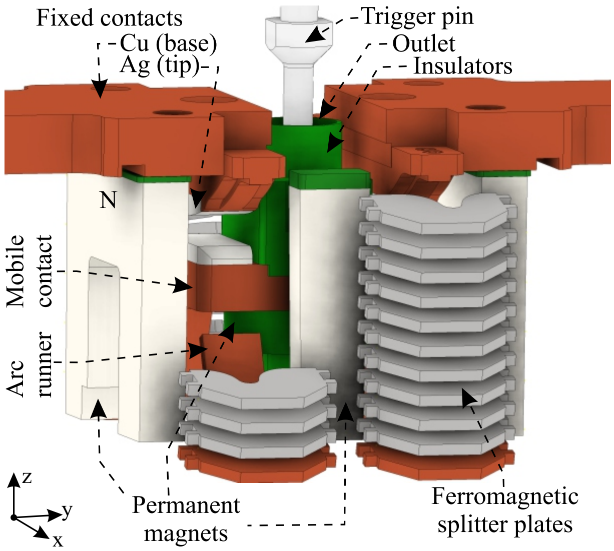

Figure 2. Inner layout of the contactor design; outer housing is dismissed for visualization purposes

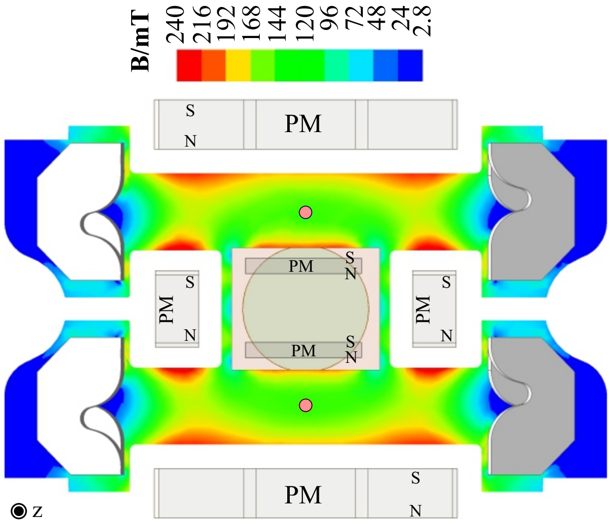

Figure 3. Top view of the magnetic field distribution created by the permanent magnets (PM) inside the arcing chamber on a xy-plane situated 1mm above the mobile contact

currents impose significantly shorter switch-off durations, typically on the order of few milliseconds depending on the specific network configuration [3, 4]. Nevertheless, it is important to note that the contactor described in this publication is intended for the switch-off process under nominal voltage, i.e. 800 V_{DC},and nominal, i.e. 250 A, or moderately over-current conditions. Each contactor contains two breaking units designed to interrupt at 400 V_{DC} and each unit has a double break structure with fixed and mobile arcing contacts, made from a copper base and silver tips, and four arcing chambers with ferromagnetic splitter plates. The contactor case, not shown in Figure 2 for better visualization of the arcing chambers, has PA66 walls and remains predominantly closed, with the exception of a minor opening surrounding the trigger pin.

To optimize the displacement of the electric arc and minimize the total commutation time, a very important feature of this design is the integration of permanent magnets positioned around the arcing contacts and along the arc runners, as shown in Figure 2. All permanent magnets are positioned inside the contactor case to protect them from the thermal stress generated by the electric arc. The preliminary analysis of the magnetic field distribution within the arcing chamber revealed significant spatial variability, as illustrated in Figure 3. The regions proximal to the contactor case walls, where the permanent magnets are located, exhibit a magnetic field strength ranging from 200 mT to 240 mT. In contrast, the central regions show a reduction in magnetic field strength to approximately 120 mT.

The experimental setup designed for the contactor testing consists of a sealed chamber used to test the contactor interruption process and arcing conditions at different altitudes, an external circuit to generate the test currents, several measurement devices, and a specialized circuit for controlling the device under test and the measurement trigger sequence.

3. Numerical model

As described in section 2, within the context of this particular application, an accurate representation of the magnetic field computation is imperative. While magnetic field effects are incorporated into numerous magnetohydrodynamic (MHD) numerical models, the majority of these models often simplify this consideration. Simplifications are performed by either assuming a uniform magnetic field throughout the computational domain [5] or adopting simplified material parameters for ferromagnetic parts present in the computational domain. Only a limited number of numerical models, e.g. [6], consider a dedicated solver for the computation of the electromagnetic field distribution.

The numerical model developed to facilitate the contactor research within the HECATE project addresses this challenge by connecting and transferring data between two dedicated solvers developed by Ansys Inc. The first solver, handling the fluid-dynamics component is represented by Fluent, a well-established and robust finite volume solver utilized for the simulation of electric arc phenomena. The second computational solver is represented by Maxwell 3D, part of the Ansys Electronics Desktop suite. This finite element solver is used to calculate the electromagnetic aspects for this MHD problem. The communication and the data transfer between the two solvers is managed by the Ansys Coupling interface, a general purpose package developed by Ansys for coupling independent physics solvers into multiphysics simulations.

To optimize computational time, the contactor geometry was adapted for numerical modeling by eliminating or reconfiguring specific elements considered to

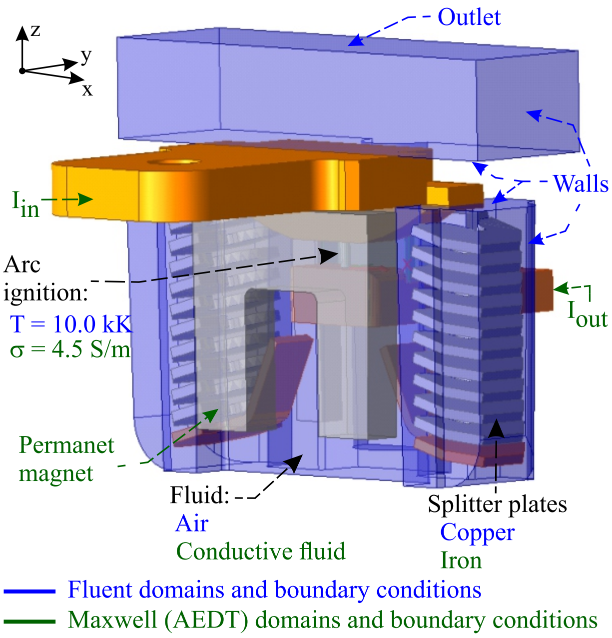

Figure 4. Numerical model domains and boundary conditions for Fluent and Maxwell

have a minimal impact on the overall flow dynamics of the electric arc. Additionally, given that the two arcing chambers depicted in Figure 2 are linked by a single narrow opening, assumed to have a minimal impact on flow dynamics within the arcing volume, the initial phase of the modeling process focused only on modeling a single arcing chamber along with its associated components. The final geometry used for the numerical modeling discussed in this paper is depicted in Figure 4.

The subsequent sections will detail the setup selected for each solver. However, prior to this, some general remarks concerning this model will be given:

- As the model is solved using two distinct software environments, it was mandatory to adapt several geometry elements and the boundary conditions to align with the requirements of each solver. This implies that not all physical elements described in Figure 4 need to be included in the problem definition of both solvers. Only the domain of interest where the data transfer occurs, i.e. the Fluid domain in Figure 4 has to be present for both solvers;
- The configuration of the model's physics, particularly within the Fluent setup, is maintained at a moderate level. This decision is attributed to the focus on the solvers coupling and the subsequent increase in complexity that this coupling introduces;
- The model presented in this publication is valid only for ground-level conditions, i.e. the pressure outside the device is considered to be atmospheric pressure.

3.1. Fluid domains setup

The hydrodynamic solution of the numerical model is computed using Ansys Fluent, where, in addition to the gas flow dynamics, the model also solves for the energy transport. The system of equations includes the influence of the Lorentz force (F_L), the Joule heating (P_j), the radiation losses (q_{rad}) and is characterized by the following system of equations:

- Mass conservation:

$$\frac{\partial \rho}{\partial t} + \vec{\nabla} \cdot (\rho \vec{v}) = 0 \quad (1)$$

- Momentum conservation:

$$\frac{\partial \rho \vec{v}}{\partial t} + \vec{\nabla} \cdot (\rho \vec{v} \cdot \vec{v}) = \vec{\nabla} \cdot (\eta \vec{\nabla} \vec{v}) - \vec{\nabla} p + F_L \quad (2)$$

- Energy conservation:

$$\frac{\partial \rho H}{\partial t} + \vec{\nabla} \cdot (\rho H \vec{v}) = \frac{\partial p}{\partial t} + \vec{\nabla} \cdot \left(\frac{\lambda}{c_p} \vec{\nabla} H \right) + P_J - q_{rad} \quad (3)$$

In the presented approach, the Lorentz force and Joule heating values, present in the momentum and energy equations, are imported from the electromagnetic solution via the Ansys System Coupling, as described in subsection. 3.3. The Fluent solution includes beside the Fluid computational domain also the electric contacts, the splitter plate system, and the arc runners as solid domains; however, the heat transfer from the fluid to these solid domains is currently constrained. The Fluid domain from Figure 4 is modeled as air with its viscosity, thermal conductivity and electric conductivity varying as a function of temperature and pressure [7], specific heat set as a function of temperature for atmospheric pressure and the density set by the ideal-gas equation. The Fluid domain is enclosed by walls and includes a single outlet where an atmospheric boundary condition with a temperature of 300 K is imposed. The radiation losses, q_{rad} in (3), are treated using the net emission coefficients (NEC) method with values according to [8] for a radius of 0.1 mm as a function of temperature for atmospheric pressure. The arc initialization is achieved by patching a cylindrical region of radius 0.5 mm, located at the center of the stationary and mobile contacts, with a temperature of 10 000 K.

3.2. Electromagnetic domains setup

The electromagnetic solution of the model is computed by the Ansys Electronics Desktop Maxwell 3D magnetostatic solver that solves the following Maxwell equations [9]:

$$\nabla \times \vec{H} = \vec{J} \quad (4)$$

$$\nabla \cdot \vec{B} = 0 \quad (5)$$

with the constitutive material relationship:

$$\vec{B} = \mu_0(\vec{H} + \vec{M}) = \mu_0 \mu_r \vec{H} + \mu_0 \vec{M}_p \quad (6)$$

where $\vec{H}$ represents the magnetic field strength, $\vec{B}$ the magnetic flux density, $\vec{J}$ the current density, $\vec{M}$ the permanent magnetization and μ_0 and μ_r the vacuum and relative permeability. The resulting electromagnetic force generated on a current carrying conductor in a magnetic field is computed using (7), while the Joule heating are computed using (8).

$$\vec{F}_L = \int_{Vol} \vec{J} \times \vec{B} \, dV \tag{7}$$

$$P_J = \int_V (\vec{E} \cdot \vec{J}) \, dV \tag{8}$$

In Maxwell, the Conductive Fluid domain from Figure 4 overlaps, from a geometric point of view, with the Air domain defined in Fluent and is considered a static fluid with spatially dependent electric conductivity defined according to the values received from Fluent through the Ansys System Coupling. The input current, in this case 200 A due to the initial project requirements, is set on the outer edge of the fixed contact while the current output is set on the outer edge of the mobile contact. The conductive path, required for the model initialization, is closed through a conductive cylinder positioned between the stationary and mobile contacts. The permanent magnets are characterized by a magnetic coercivity of $820\,000\,\mathrm{A\,m^{-1}}$, whereas the ferromagnetic splitter plates consider a nonlinear magnetic permeability set according to a predefined B-H curve provided by the manufacturer. The entire model is enclosed by a vacuum region, not represented in Figure 4, used exclusively for the electromagnetic field calculations.

3.3. System coupling setup

The integration of the two solvers is facilitated by Ansys System Coupling, a general-purpose interface designed to connect two or more physics solvers within a multiphysics analysis. In this specific case, it enables the exchange of heat losses and Lorentz forces, computed by Maxwell, and electric conductivity and temperature, computed by Fluent as described in Table 1. The data coupling takes place within the Fluid region, including the arc ignition region.

	Source	Target	Variable
1.	Fluent	Maxwell	Electric Conductivity (σ)
2.	Fluent	Maxwell	Temperature (T)
3.	Maxwell	Fluent	Lorentz Force (F_L)
4.	Maxwell	Fluent	Heat Rate (P_J)

Table 1. Ansys System Coupling data transfer

An effective data transfer between the two solvers requires a relatively good overlap between the mesh defined in Fluent and Maxwell. It is important to consider this aspect because, in this case, two distinct mesh types will be generated. The Fluent mesh is defined prior to the computation and remains static throughout the entire solving process. Conversely, the Maxwell mesh is initialized with user defined values that are used to generate an initial mesh that undergoes local refinement during the solving process. For the case analyzed in this publication, in Fluent was defined a tetrahedral mesh with approximately 700000 elements and different degrees of refinement for the areas where higher gradients were expected, e.g. arc ignition, splitter plates surroundings. The mesh set in Maxwell has an initial number of approximately 80000 elements and to reach convergence will usually perform a 3 step refinement increasing the mesh density up to approximately 160000 elements. With these settings, a mapping of more than 94 % is achieved for the data sent from Fluent to Maxwell and above 99 % for the data sent from Maxwell to Fluent.

The model was solved in transient mode with a total duration of 1.5 ms using a variable time step for numerical stability reasons. All computations were performed on an HPC cluster using 48 to 64 cores for Fluent and 4 to 8 cores for Maxwell.

4. Results

The results presented in this publication should be considered primarily qualitative for two main reasons. One reason relates to the experimental program that is conducted using a fully developed prototype that does not allow a good separation of effects or, in some cases, specialized observations. The second reason relates to the simulation model that, as mentioned in section 3, has a moderate complexity and remains under development, requiring the implementation and refinement of certain physical effects, e.g. radiation modeling or electrode movement, before conducting a proper qualitative comparison with the experimental data.

4.1. Experimental results

The experiments performed by our project partners from Safran Electric and Power, within a pressurized chamber demonstrate a reliable arc quenching procedure at different altitudes up to 16.7 km. The arc quenching duration is $\approx$ 1.5 ms at ground level, $\approx$ 2.5 ms at 13.7 km (45 kft), and $\approx$ 2.8 ms at 16.7 km (55 kft). According to the preliminary analysis of the experimental results, we have observed four main phases of the arc development from its inception to its quenching. The stages were defined as:

- ☐ Phase 1: represents the formation of the arc column in the time interval starting from the initial onset of the arc to the formation of a fully developed arc column;
- ☐ Phase 2: defined as the contact phase, denotes the time interval when the arc is accelerated from its initial position up to the time when it reaches the outer edge of the mobile contact;
- ☐ Phase 3: defined as the expansion phase, represents the time interval when the arc elongates and moves from the edge of the mobile contact onto the arc runner;

☐ Phase 4: or the splitter phase, defined by the time interval when the arc enters the splitter plate system until its quenching.

For the experiments at ground level, representative for the comparison with the numerical model, initial observations suggest that the arc exhibits a static behavior during Phase 1 that has a duration of ≈ 0.5 ms. Conversely, upon the establishment of the arc column and the initiation of Phase 2, the arc exhibits an extreme acceleration that moves the arc almost to the edge of the contact within ≈ 0.09 ms to ≈ 0.12 ms followed by a deceleration period up to ≈ 0.2 ms when the Phase 2 ends. Phase 3, with a duration of ≈ 0.5 ms, is characterized by a certain delay in the arc displacement before moving on the arc runner. During the final phase, with a duration of ≈ 0.3 ms, the arc presents an efficient propagation and interaction with the splitter plate system, resulting in an effective quenching. Nonetheless, the results presented herein should not be considered definitive, as they are subject to additional enhancements that are foreseen in the experimental program.

Another noteworthy observation from the post-experiment contact analysis indicated that the arcing contacts exhibited regions with significantly higher erosion relative to their adjacent areas. This behavior is illustrated in Figure 5 where two distinct post-arcing structures are visible. The first structure, delineated in red, exhibits a contact surface area with significant material erosion. In contrast, the second region, delineated in blue, presents evidence of arc or plasma interaction with significantly less material erosion. These areas, positioned towards the contactor case wall, represent regions of direct and indirect interaction between the arc and the electrical contact. It can be inferred that during the contact phase, following its formation, the arc moves towards the contact edge under the influence of the electromagnetic forces. Towards the end of this phase and the beginning of the expansion phase, the arc presents a stagnation period causing high material erosion of the contacts and imposing substantial thermal stress upon all nearby components.

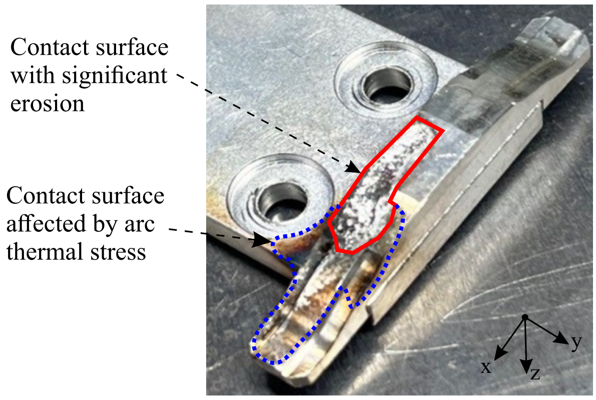

Figure 5. Contact erosion due to arcing in experiments conducted with a real contactor

4.2. Simulation results

The simulation results, presented in the following, focus mainly on the Phase 2 up to the point where the arc column elongation starts at the beginning of Phase 3, as defined in section 4.1. The intention is to provide, from a simulation perspective, theoretical explanations for the dynamics of the arc movement and the experimentally observed contact erosion.

In Figure 6 the simulation results for two different time steps considered relevant for the interpretation of the experimental observations are presented. The images mark the arc position by plotting the 10 000 K (orange) and the 7000 K (green) temperature isotherms along with the flow velocity vectors (blue) and the pressure wave formed by the arc expansion (grey).

The arc is initialized at a central location between the two open contacts as illustrated in Figure 6a by the dotted circle and lines. Due to the initial contact separation, the arc channel expands rapidly and generates a pressure wave in both positive and negative x-directions. As a consequence of the arc initialization and the fast column expansion, the electromagnetic forces induced by the permanent magnets will exert, almost instantly, a significant force that accelerates the arc column in the positive x-direction. For this specific case, given a contact distance of 1.7 mm, the mean electromagnetic force exerted on the arc column is approximately 130 mN. Under these conditions, the arc will present at first an strong acceleration, that moves its column close to the contact edge within 70 μs, a time interval with ≈ 30 % lower than the one observed in the experiments. Within this time interval, the arc remains relatively well centered between the contacts and its forward acceleration is sustained by both the electromagnetic forces and the fluid dynamics, i.e. the majority of the fluid velocity vectors are oriented in the positive x-direction.

Subsequent to this stage, the pressure wave, having propagated to the rear of the splitter plate system, initiates a reverse flow directed towards the arc column. As it increases, this reverse flow counteracts the electromagnetic forces, resulting in a deceleration of the arc column's movement. A secondary effect created by the fluid dynamics relates to the displacement of the arc column towards the outer wall of the arcing chamber as the flow propagates towards the lower pressure regions, e.g. outlet and left hand side of the arcing chamber. In the near wall region, the arc column will be subjected to higher magnetic forces, see Figure 3, that will enhance the electromagnetic force in the negative y-direction. According to our observations, these cumulative effects will modify the force distribution on the arc column, resulting in a stagnation period for the arc at contact edge. In the numerical model up to ≈ 150 µs that, most likely, is responsible for the higher material erosion.

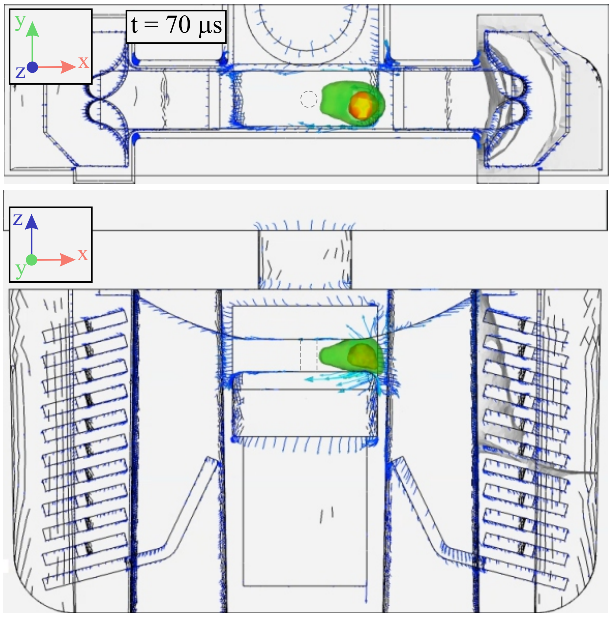

(a) . Arc position and flow development at 70 µs

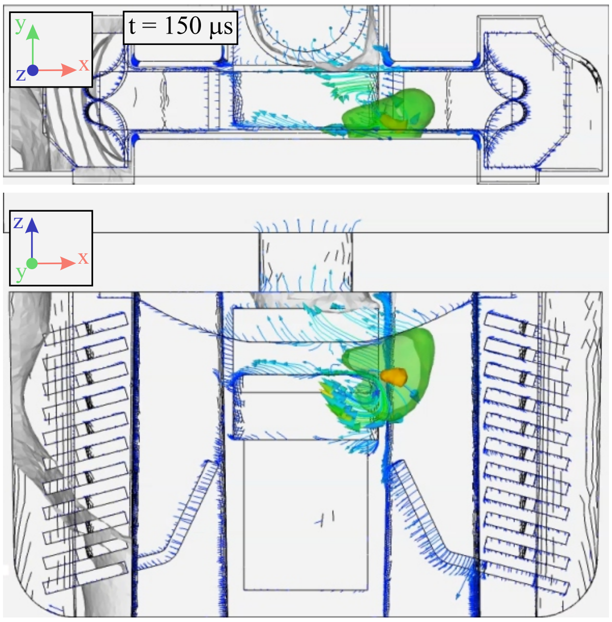

(b) . Arc position and flow development at 150 µs

Figure 6. Up and side view of the arc position, fluid velocity vectors and pressure wave inside the arcing chamber at different time steps

5. Conclusions

In this publication, we have conducted an analysis of both experimental and numerical findings related to the development of a contactor used for the protection of the KHVDC system for hybrid regional aircraft. The experimental program demonstrated the capability of the contactor to interrupt nominal currents at varying altitudes but it also revealed significant material erosion and increased thermal loads in specific regions of the device. The numerical model used the multiphysics capabilities of the Ansys suite to create a bidirectional coupling between the fluid-dynamic and electromagnetic solvers over the domains of interest improving the treatment of non-linear magnetic field distribution for the presented contactor. The model showed the effect of the hydro-dynamic and electromagnetic force distribution on the arc column dynamics and explained in a qualitative manner the experimental observations. These results are relevant for the future development of this contactor that will take place by enhancing both the experimental and numerical model in a coupled manner.

Acknowledgements

The authors would like to thank Dipl.-Ing. Kevin Enouf, Dipl.-Ing. Guillaume Prieur and Dr. Lucas Fuster from Safran Electric and Power for providing the experimental data and for their valuable discussions during this project.

The authors would like to thank the HECATE Project, funded by the European Union under GA no 101101961-HECATE. Views and opinions expressed are, however, those of the author(s) only and do not necessarily reflect those of the European Union or Clean Aviation Joint Undertaking. Neither the European Union nor the granting authority can be held responsible for them. The project is supported by the Clean Aviation Joint Undertaking and its members.

References

[1] HECATE project:. available online: https://hecate-project.eu.

[2] D. Izquierdo, G. Casas, A. G. Garriga, et al. Electrical Distribution System LCA for Future Regional Aircraft—Preliminary Definition of Methodology. 10(11):920, 2023. doi:10.3390/aerospace10110920.

[3] B. Barbu, J. Jebramcik, K. Fuchs, et al. DC-Switching principles from Low Voltage to High Voltage. In *VDE-Fachtagung Hochspannungstechnik 2016: 14-16 November 2016, Berlin, Germany*, volume 150 of *ETG-Fachbericht*, pages 54–59. VDE Verlag GmbH. ISBN 3-8007-4310-8.

[4] A. Sauer. *The DC-factory: Energy Efficient. Robust. Forward-looking.* Hanser, 2021. ISBN 978-3-446-47174-0.

[5] J. J. Shea, E. Heckman, and J. C. S. Guevara. DC Arc Properties in a DC Magnetic Field. In *2018 IEEE Holm Conference on Electrical Contacts*, pages 195–203. ISSN 2158-9992. doi:10.1109/HOLM.2018.8611725.

[6] C. Rümpler. *Lichtbogensimulation Für Niederspannungsschaltgeräte*. PhD thesis, Technische Universität Ilmenau, 2009.

[7] A. D'Angola, G. Colonna, C. Gorse, and M. Capitelli. Thermodynamic and transport properties in equilibrium air plasmas in a wide pressure and temperature range. 46(1):129–150, 2008. doi:10.1140/epjd/e2007-00305-4.

[8] Y. Naghizadeh-Kashani, Y. Cressault, and A. Gleizes. Net emission coefficient of air thermal plasmas. 35(22):2925, 2002. doi:10.1088/0022-3727/35/22/306.

[9] Ansys Inc. Ansys Electromagnetics Suite 2024 R1 - Maxwell Help, 2024.